Published in final edited form as:
Mol Imaging. 2008 ; 7(3): 118–131.

Optical imaging of matrix metalloproteinase-7 activity *in vivo* using a proteolytic nanobeacon

Randy L. Scherer[1,3], **Michael N. VanSaun**[1], **Oliver McIntyre**[1,2], and **Lynn M. Matrisian**[1,2,3]

[1]Department of Cancer Biology, Vanderbilt University, Nashville TN 37232-6840

[2]Vanderbilt-Ingram Cancer Center, Vanderbilt University, Nashville TN 37232-6840

[3]Department of Interdisciplinary Materials Science and Engineering, and Vanderbilt University Institute of Imaging Science, Vanderbilt University, Nashville TN 37232-6840

Abstract

Matrix metalloproteinases (MMPs) are extracellular proteolytic enzymes involved in tumor progression. We present the *in vivo* detection and quantitation of MMP7 activity using a specific near-infrared polymer-based proteolytic beacon, PB-M7NIR. PB-M7NIR is a pegylated polyamidoamine PAMAM-Generation 4 dendrimer core covalently coupled to a Cy5.5 labeled peptide representing a selective substrate that monitors MMP7 activity (S, sensor), and AF750 as an internal reference to monitor relative substrate concentration (R, reference). *In vivo* imaging of tumors expressing MMP7 had a median S/R ratio 2.2-fold higher than a bilateral control tumor. *Ex-vivo* imaging of intestines of multiple intestinal neoplasia (APC^{Min}) mice injected systemically with PB-M7NIR revealed a 6-fold increase in S/R in the adenomas of APC^{Min} mice compared to control intestinal tissue or adenomas from MMP7-null Min mice. PB-M7NIR detected tumor sizes as small as $0.01cm^2$, and S/R was independent of tumor size. Histological sectioning of xenograft tumors localized the proteolytic signal to the extracellular matrix; MMP7-overexpressing tumors displayed an approximately 300-fold enhancement in S/R compared to non-expressing tumor cells. In APC^{Min} adenomas, the proteolytic signal co-localized with the endogenously-expressed MMP7 protein with S/R ratios approximately 6-fold greater than that of normal intestinal epithelium. PB-M7NIR provides a useful reagent for the *in vivo* and *ex-vivo* quantitation and localization of MMP-selective proteolytic activity.

Keywords

near infrared; dendrimer; MMP; in vivo imaging

Introduction

One of the defining characteristics of malignancy is the ability of cancer cells to metastasize and invade distant organ sites. Proteolysis of the extracellular matrix (ECM) is required to accommodate increased growth, migration, and invasion of tumor cells. Matrix metalloproteinases (MMPs) are a family of extracellular, zinc-dependent proteinases that are capable of degrading most of the multiple components of the ECM (1). In the tumor microenvironment, host and tumor derived MMPs are often misregulated leading to uncontrolled degradation of the ECM. Of the 24 identified human MMP gene products,

Corresponding author: Lynn M. Matrisian, Ph.D., Professor and Chair, Department of Cancer Biology, 2220 Pierce Ave, 771 Preston Research Building, Vanderbilt University, Nashville TN 37232, (615) 343-3413, FAX (615) 936-2911, Lynn.Matrisian@vanderbilt.edu.

MMP7 is one of the smallest members of this family possessing only the domains necessary for targeting to the secretory pathway, control of latency, and catalytic activity. MMP7 is notably produced by cells of epithelial origin and contributes to tumor formation in a number of epithelial-derived adenocarcinomas (2,3). From a molecular imaging standpoint, MMP7 is a secreted extracellular proteinase that appears to be a promising target for *in vivo* detection of tumors and quantitative analysis. Thus, MMP7 provides an attractive target for developing an enhanced near-infrared (NIR) proteolytic beacon (PB) to non-invasively assess proteolytic activity.

Quenched fluorescent peptide probes have been used for decades to measure proteolytic activity of purified enzymes, and quenched fluorescent matrix proteins have been applied to cell culture models to monitor extracellular proteolysis (4). Small molecule activity-based probes have been used in both in vitro and in vivo studies to monitor cysteine and serine proteinase activities (5), but have not yet proven to be useful for measuring MMP activity. The ability to probe tissue with light for minimal/non-invasive detection of cancer has become feasible mainly due to the development of fluorescent probes emitting in the near-infrared spectrum where tissue has both low absorption and reduced scattering (6). A number of different fluorescent approaches have demonstrated the capability to detect specific molecular events *in vivo* (7–10). For optical imaging, Achilefu and colleagues have prepared a number of NIR optical contrast agents designed to either bind to or be metabolized by tumors and, together with Chance, has demonstrated the feasibility of detecting 2-cm deep subsurface tumors using a metabolism-enhanced NIR fluorescent contrast agent and NIRF *in vivo* imaging (11–13). Weissleder and colleagues have utilized NIR probes to assess proteolytic activity and subsequent inhibition by MMP inhibitors (5,6). The Tsien's group described a new strategy using protease activatable cell-penetrating peptides to deliver fluorescent labels within tumor cells(14). Probes have been developed to assess proteolytic activity based on Förster resonance energy transfer (FRET): endogenous quenching of closely positioned fluorochromes on peptide substrates that upon proteolytic cleavage produce enhanced fluorescence (15–17). In particular, Pham and others have developed an MMP7 NIR probe that was capable of imaging protease activity *in vitro* (18). Thus, the principle to detect proteolytic activity *in vitrol vivo* has been demonstrated.

We previously described a polymer-based fluorogenic peptide substrate that selectively detected MMP7 activity *in vitro* and *in vivo* with fluorophores that emit in the visible range (15). The fluorogenic peptide substrate is built on a generation 4-polyamidoamine (G4-PAMAM) backbone containing a non-cleavable internal reference fluorophore that monitors both the cleaved and uncleaved reagent. In the present study, we utilized NIR FRET pair fluorochromes to increase the efficiency of light traveling through tissue (19). These new reagents, referred to as PB-M7NIR to indicate they are proteolytic beacons (PB) selective for MMP7 (M7) that emit in the near infra-red range (NIR), extend our previous studies to examining MMP7 activity in the context of multiple *in vivo* and *ex vivo* tumor microenvironments, as well as to provide quantitative assessment of relative proteolytic activity.

Materials and Methods

Materials

All chemicals and biochemicals were reagent-grade and solutions were prepared in deionized filtered water (Milli-Q, Billerica, MA, USA). Generation 4 Starburst® PAMAM dendrimer (10% w/w in methanol), Brij® 35 solution (30% w/v) and Tricine (>98%) were obtained from Sigma-Aldridge (St. Louis, MO, USA). PEG5000 was obtained from Shearwater Polymers, Inc (Shearwater, TX, USA). SIA (N-succinimidyl iodoacetate) was obtained from Pierce Chemical (Rockford, IL, USA). M7 [(AHX)-RPLALWRS-(AHX)-C,

where AHX is aminohexanoic acid], a HPLC-purified peptide that includes two AHX linkers was obtained from Open Biosystems (Huntsville, Al, USA). The N-hydroxysuccinimidyl (NHS) ester derivatives of Cy5.5 and AF750, two near-infrared fluorophores were obtained from GE Healthcare (London, United Kingdom) and Molecular Probes, Invitrogen (Carlsbad, CA, USA), respectively. MMP7 was obtained from Calbiochem (San Jose, CA, USA). Low Fluorescent (TD-97184) and high fat chow (TD-5015) were obtained from Harlan Teklad (Madison, WI, U.S.A.)

Synthesis of PB-M7NIR

The polymer-based fluorogenic substrate PB-M7NIR was synthesized according to the procedure outlined in Figure 1A.

Labeling M7Peptide with Cy5.5—The Cy5.5-labeled peptide, Cy5.5-M7, was designed for selective cleavage by MMP7 to yield a relatively insoluble fluorescent labeled N-terminal fragment that includes an AHX linker (Scheme 1). In the first step of synthesis, a methanolic solution (5mM) of the M7 peptide was reacted with 0.8 equivalents (eq) of Cy5.5-NHS in DMSO (7 mM) and triethylamine added to 1% (v/v) to fluorescently label the peptide at the N-terminal amine. After overnight reaction at ambient temperature, residual NH_2 groups were blocked using NHS-acetate (20 mg/ml in 2.5 eq/peptide) for 1 hr followed by glycine (2M in H_2O at 2eq/acetate) to quench residual NHS-acetate. Dithiothreitol (2 mg/ml in methanol, 0.15 eq) was then added to the reaction mixture to reduce the sulfhydryl groups on the C-terminal cysteine of Cy5.5-M7.

Coupling Cy5-M7 to G4-PAMAM-PEG—G4-PAMAM-PEG was prepared by reacting an aliquot of the PAMAM stock solution (in methanol) with an equimolar equivalent of NHS-PEG5000 (dissolved at 22 mM in methanol). The addition of PEG was required to improve the solubility of PB-M7NIR, a modification that was not required in the original PB-M7VIS (13). To synthesize the thioether-bonded conjugate $(Cy5.5\text{-}M7)_m$-PAMAM-PEG5000, the PAMAM-PEG conjugate was first activated by treatment with SIA (8 mg/ml methanol, 20 eq/PAMAM). After reaction for 20min at ambient temperature, the SIA activated PAMAM-PEG was immediately reacted with the reduced Cy5.5-M7 peptide in methanolic solution (8 peptides/PAMAM) and allowed to react at ambient temperature (24 hr in the dark) with gentle mixing. The reaction mixture was then diluted 10-fold with aqueous 0.1 mM EDTA (pH 8, previously treated with 1mM phenylmethylsulfonylfluoride) and then concentrated and purified by at least three rounds of diafiltration (CentriPrep YM-10, Millipore) followed by concentration. The fraction of Cy5.5-M7 incorporated into the peptide-PAMAM-PEG5000 co-polymer (>95%) was calculated from the relative Cy5.5 concentration in the reaction mixture versus effluents. The product $(Cy5.5\text{-}M7)_8$-PAMAM-PEG5000 (~90% based on the ninhydrin assay) was stored (4°C) at approximately 1 mg PAMAM/ml overnight and subsequently labeled with AF750 as described below.

Coupling of AF750 to $(Cy5\text{-}M7)_8$-PAMAM-PEG5000—To label the PAMAM scaffold of $(Cy5.5\text{-}M7)_8$-PAMAM-PEG5000 with AF750, the peptide-PAMAM co-polymer was made 50 mM in Na_2CO_3 (pH 9) and reacted with up to eight equivalents of AF750-NHS (7mM in DMSO). After overnight incubation at ambient temperature (22–24°C in the dark), the reaction mixture was diluted 10-fold with aqueous 0.1 mM EDTA (pH 8) and the product $(Cy5.5\text{-}M7)_8$-PAMAM-(PEG5000)$(AF750)_n$ was separated from unincorporated AF750 by diafiltration (as above) using a total of 4 washes with the same buffer. Incorporation of AF750 was calculated from absorbance at 750nm with a concentration determined to be 6 AF750/PAMAM. The final product $(Cy5.5\text{-}M7)_8$-PAMAM-(PEG5000)$(AF750)_6$, now referred to as PB-M7NIR, was stored in the dark at 4°C in 0.1 mM EDTA (pH 8) until administration after dilution into sterile saline.

Fluorescence spectroscopy

Fluorescence excitation and emission spectra of PB-M7NIR, diluted with deionized water (0.05–0.1 μM) to obtain an absorbance of <0.05, were measured in 4 mm × 4 mm quartz cuvettes at 25°C using an L-format Quanta Master QM-9 photon counting fluorimeter (1 nm steps, 2 nm slits) operated with Felix software (Photon Technology International, Lawrenceville, NJ, U.S.A.). Fluorescence spectra of PB-M7NIR and subsequent controls were recorded before and after treatment with MMP7 and are illustrated with the same amplitude after cleavage to account for differences in the fluorescence concentration of each sample. MMP cleavage was determined as previously described (15). Activity of purified human liver cathepsin B and cathepsin L, both from Athens Research and Technology (Athens, GA), towards the peptide in PB-M7NIR was tested using 0.5 mM PB-M7VIS in 50 mM sodium citrate buffer (pH 5.0), 5 mM EDTA and 10 mM DTT (20). Both cathepsins B and L were active in this buffer towards DQ-collagen (10 μg/ml).

Cell Culture

SW480 human colon cancer cells were obtained from A.T.C.C. (Manassas, VA, U.S.A.). Stable clones expressing the neomycin selection cassette (SW480neo) or neomycin and MMP7 (SW480mat) were isolated and characterized as reported previously(21). Cells were maintained in Dulbecco's modified Eagles's medium containing 10% (v/v) fetal calf serum at 37°C in a 5% CO_2 environment.

In vivo Imaging of xenograft model

SW480neo control and MMP7-expressing SW480mat colon cancer cells (1×10^6 cells) were seeded on the flanks of athymic nude mice (n=13) (Harlan, Indianapolis, IN, U.S.A.). Tumors of approximately 5–10 mm in size developed after 3–4 weeks of growth. Mice were placed on a low-fluorescent diet one week post injection of cells to reduce autofluorescence particularly from the intestinal region. After 4 weeks of tumor growth, mice were anesthetized using 2% isofluorane and imaged using a cryogenically cooled CCD camera, IVIS 200 Imaging System by Xenogen (Alameda, CA, USA), in the Cy5.5 (Sensor-Cy5.5) and ICG (Reference-AF750) channels. PB-M7NIR (1.0 nmol in 100ul of sterile 0.9% saline) was retro-orbitally injected and animals were imaged for up to 30min post injection. Additional image sets of animals were recorded every hour for up to 4 hrs post injection of PB-M7NIR. *In vivo* results were from thirteen animals, each bearing control and MMP7-expressing xenograft tumors with *ex vivo* data from tumors removed from four of the same animals. All animal experiments were in accord with IACUC regulations. The imaging data sets were analyzed using Living Image® software by Xenogen in the Cy5.5 and ICG channels that predominately measure Cy5.5 (sensor) and AF750 (reference) fluorescence respectively. Regions of interest were created to measure the average radiance (photons/sec/cm^2/steradian) both pre and post injection of PB-M7NIR in the tumor bearing regions and in the hind leg of the mouse (muscle tissue) for use as normal tissue control. Sensor and reference signal is measured either as signal above pre-injection background and/or signal minus background post-injection as indicated.

Ex-vivo Imaging of intestinal adenomas

Four congenic C57Bl/6-Min (Min/+) mice positive for the Apc^{Min} allele (Jackson Laboratory, Bar Harbor, ME, USA), three congenic C57Bl/6-Min-MMP7-null mice (22), and four C57Bl/6 normal control mice (Jackson Laboratory, Bar Harbor ME, USA) were placed on a high fat diet 5015 (Harlan Teklad) for fifteen weeks and then on low fluorescent chow (TD-97184, Harlan Teklad) for two weeks to reduce tissue autofluorescence. Mice were anesthetized using 2% isofluorane and retro-orbitally injected with PB-M7NIR (1.0nmol in 100ul sterile saline 0.9%). Approximately 1 hr post injection, animals were

sacrificed using CO_2 asphyxiation at which point their small intestine (duodenum, jejunum, ileum), cecum, and colon were removed, rinsed with ice-cold 1X phosphate buffer saline (50 ml), and opened longitudinally to reveal adenomas on the luminal surface. Images were taken in the Cy5.5 (Cy5.5-sensor) and ICG (AF750-reference) channels using a cryogenically cooled CCD camera (IVIS 200 Imaging System, Xenogen, Alameda, CA, U.S.A.) to examine fluorescence signal from MMP7 cleavage. The tumor and non-tumor image data sets were analyzed using Living Image software by Xenogen to measure fluorescence intensities in regions of interest. Signal was recorded as average radiance (photons/second/cm^2/steradian) for both channels and calculated as signal minus background intensity.

Histological Imaging of proteolytic activity

Xenograft tumors or intestinal adenomas were each resected, placed in optimal cutting temperature (OCT) embedding media, snap frozen in liquid nitrogen, and stored at −20°C until sectioned (5–10μm) using a cryomicrotome. For histological analysis, OCT was removed from the samples by immersing the slides in H_2O followed by 70% EtOH. Slides were aqueously mounted (Biomeda, Foster City, CA, USA) in media containing 4',6-diamidino-2-phenylindole (DAPI, 2μM). Quantitative fluorescence imaging was done by taking digital pictures with full-frame, black and white CCD camera (MicroMax 1317-K1; Princeton Instruments, Trenton, NJ, U.S.A.) coupled to a fluorescence microscope with a variety (10X, 20X, and 40X-oil immersion) of Plan-Neofluar objective lenses (Axiophot; Carl Zeiss, Thornwood, NY, U.S.A.). Camera control, image acquisition and analyses were performed using Metamorph imaging software (Universal Imaging, Downingtown, PA, U.S.A.). Fluorescence signal was linear with camera exposure time, and the exposure conditions were optimized for maximum dynamic range. White light and DAPI images were used to focus and orient the specimen field before fluorescence excitation. At least two images were then acquired for optimal excitation. Light was collected using the 40X objective lens under oil immersion. Fluorescence *sensor* signal (Peak Emission 694 nm) was discriminated using a Cy5.5 near infrared band-pass filter set (Chroma Technology Corp., Brattleboro, VT, U.S.A.) from *reference* fluorescence signal (Peak Emission-776 nm) using a Cy7 band-pass filter set (Chroma Technology Corp., Brattleboro, VT, U.S.A.). The intensity in each channel was calculated as the average counts/pixel after subtraction of background signals from control samples (non-tumor bearing C57Bl/6 intestine).

Immunohistochemistry

Spontaneously occurring intestinal polyps were harvested from *Min*/+ and *Min*-7-null mice, along with normal intestinal tissue harvested from C57Bl6 normal mice, frozen in OCT, and used to generate 5-μm sagital sections. Sections were rinsed in a series of graded alcohols to remove the OCT, rehydrated, incubated in 0.6% hydrogen peroxide for 30 minutes to remove endogenous peroxidase activity, and heated to 95°C for 3.5 minutes in 10 mM citrate buffer, pH 6.0, to reveal antigenic epitopes. Blocking was performed by incubating for 1 hour at room temperature in a solution containing 5% goat serum, 1% bovine serum albumin, 0.5% Tween-20 and 0.1 M MgCl2 in 10 mM Tris-HCl, pH 7.4. Sections were then incubated with a rat monoclonal antibody raised against MMP7 (23) diluted 1:100 in blocking solution overnight at 4°C. The slides were washed three times in tris-buffered saline (TBS) containing 0.05% Tween-20 before incubating for 1 hour at room temperature with biotinylated rabbit anti-rat IgG (Vector Laboratories, Burlingame, CA) diluted 1:1000. After another series of washes in TBS containing 0.05% Tween-20, the sections were processed using the Vectastain Elite ABC kit (Vector) according to the manufacturer's instructions. Positive signal was detected using diaminobenzidine (Sigma, St. Louis, MO) as a chromogen and the sections were counterstained with Mayer's hematoxylin (Sigma).

Statistical Analysis

All data generated using PB-M7NIR *ex vivo* imaging assays were analyzed with a one-way ANOVA (Newman-Keuls Multiple Comparison Test) method for three sample sections or for two sample sets using a nonparametrical (Mann-Whitney) method. Data generated using the xenograft and Min models were analyzed using a nonparametrical (Mann-Whitney) method (Graph Pad Software, San Diego, CA, USA).

Results

Preparation and fluorescence properties of PB-M7NIR

PB-M7NIR was constructed on a pegylated (PEG5000) dendrimeric scaffold (Starburst®; G4-PAMAM) with both an optical protease sensor (Cy5.5-M7) and an internal reference, AF750 (Figure 1A). The peptide sequence of Cy5.5-M7 is based on a fluorogenic peptide that was optimized for MMP7 cleavage (21). Based on the results of preliminary studies, PB-M7NIR reagent was prepared to have maximum incorporation with similar equivalents of sensor and reference fluorophores for optimal self-quenching and fluorescence resonance energy transfer quenching. After preparation, absorbance taken from the optimized product compared to reaction mixture yields an average of 8 Cy5.5-M7 peptide substrates and 6 AF750 reference fluorophores per PAMAM (Figure 1B). After treating PB-M7NIR with active MMP7, the relative increase in Cy5.5 spectral amplitude yields an approximate 5-fold increase in Cy5.5-fluorescence compared to the EDTA treated control (Figure 2). In contrast, the AF750 reference fluorescence signal increases minimally upon treatment remaining virtually the same signal as the EDTA-treated control. Comparison of the amplitudes of the emission spectra of PB-M7NIR before and after treatment with MMP7 shows that the Cy5.5 fluorescence signal functions as an optical sensor to detect proteolysis of the Cy5.5-M7 peptide, whereas the AF750 fluorescence serves as an internal reference to monitor the total (cleaved and uncleaved) concentration of the reagent, consistent with the original design of this PB. The peptide in PB-M7NIR is identical to that in PB-M7VIS, which was shown to be 56-fold more active with MMP7 compared to MMP2, and 13-fold more selective for MMP7 versus MMP3 (15). PB-M7VIS was not a substrate for cathepsins B or L when tested at pH 5.0 (data not shown).

In vivo imaging of subcutaneous xenograft tumors

To evaluate the selectivity of PB-M7NIR, athymic nude mice were subcutaneously injected on either flank with a human colon cancer cell line that does not express MMP7 (SW480neo), and a cell line derived from the same parental cells following transfection with the human MMP7-cDNA (SW480mat). Both cell lines express several MMPs, including MMP9 (24), and to our knowledge differ only in the expression of MMP7. Once tumors were established, 1nmole of PB-M7NIR was injected i.v., resulting in a final concentration of approximately 0.5μM, which was calculated to be below the kD of 2μM to reduce nonspecific cleavage and optimize for MMP7 selectivity. Mice were imaged at various time points up to four hours post injection in the Cy5.5 channel to measure the Cy5.5 *sensor* signal and in the ICG channel to measure the AF750 *reference* signal (Figure 3A–D). Signal in the reference channel was highest at the first measurement after injection (1 hr) and decreased thereafter, presumably due to the clearance of the cleaved and uncleaved PAMAM-AF750 core (Figure 3E). In contrast, the sensor signal markedly increased over the first three hours consistent with MMP7 cleavage resulting in enhanced fluorescence in the Cy5.5 channel. Sensor signals varied in intensity from mouse-to-mouse; however, signal in the control tumor was always less than in the MMP7 expressing tumors in the same mouse (Table 1). To further evaluate the effective cleavage of PB-M7NIR, sensor to internal reference ratios (S/R) were calculated to assess the cleaved (sensor, S) to total substrate (reference, R) retained in the tumor; S/R ratio increased over time (Figure 3E). Using data

from the four hour time point, S/R ratios were calculated for the control neo tumor and the MMP7 expressing mat tumor (Table 1). The S/R ratio in the MMP7 expressing mat tumors ranged from 24 to greater than 1000, with an average of 275 and median of 60.8. The control neo tumor in the same animal consistently showed a lower S/R ratio (Figure 3F), but the numbers where highly variable and ranged from 1 to 293 (mean= 69.7 and median=39.2). Despite mouse-to-mouse variation, the S/R ratio in the MMP7-expressing tumors divided by the S/R ratios in the control tumor in the same mouse gave an average of 6.8 fold increase and a median of 2.2 (Table 1).

Quantitative *ex vivo* fluorescence imaging of PB-M7NIR in histological sections

To localize MMP activity in the tumor microenvironment at the cellular level, subcutaneous xenograft tumors were removed 4 hr post injection of PB-M7NIR and snap frozen prior to cryostat sectioning (z = 5 μm). Sections were aqueously mounted with DAPI and analyzed by fluorescence microscopy (Figure 4A–H). In the MMP7 positive xenograft tumors, PB-M7NIR sensor signal was predominately localized at the tumor-stroma interface with high fluorescence being detected in the ECM (Fig 4A–D). Sensor signal was not localized in the control tumors (Figure 4E–H) and remained lower than the MMP7 positive tumor signal for all mice. Sensor/reference ratios were calculated for each sample in three different regions of the tumor (Figure 4I). The S/R ratio in the MMP7 expressing tumors ranged from 600 to over a 1000, with an average of 692 and a median of 629. The control neo tumor in the corresponding animal consistently showed a lower S/R ratio with an average of 2.3 and a median of 1.9. On average, the Mat S/R ratio divided by Neo S/R ratio gave a average 355-fold increase and a median of 360 (Figure 4 I,J). It should be noted that the sensor and reference signals measured using the fluorescent microscope are in counts/sec differing from the average radiance measurements using the IVIS instrument. However, the dramatic increase in S/R ratios in the MMP7 positive tumors compared to the control tumors confirms the ability of PB-M7NIR to effectively localize and assess MMP7 activity in the tumor microenvironment.

Ex Vivo imaging of MMP7 activity in APC^{Min} mice

The sensitivity of PB-M7NIR was tested by identifying intestinal adenomatous polyps in APC^{Min} mice. APC^{Min} mice have a mutation in the adenomatous polyposis coli gene that predisposes them to develop multiple benign adenomas throughout the entire intestinal tract at an early age, mimicking the human condition Familial Adenomatous Polyposis Coli (25). The adenomas express the mRNA for several MMP family members, most notably MMP7, which localizes to the epithelial component of the tumors (22,26). MMP7 expression has been reported in early-stage, benign tumors of the gastrointestinal (GI) tract (27), and reduction in MMP7 activity specifically (22) or MMP activity generally (28) reduces the number of polyps suggesting that MMP7 represents an appropriate target for prevention strategies (29).

PB-M7NIR was administered to 15 week old APC^{Min} mice by retro-orbital injection and the mice were sacrificed 1hr post injection, the time of maximum sensor and reference signal in this model system. The intestines and colon removed and opened longitudinally displaying luminal adenomas. Adenomas were imaged under white light, Cy5.5-*Sensor*, and ICG-*Reference* channels (Figure 5A–D and data not shown). Adenomas in APC^{Min} mice demonstrated robust sensor signal, with S/R ratios averaging approximately 100 (Figure 5F & G). In contrast, the intestines of wild type mice demonstrated very little fluorescence in the sensor channel, with S/R ratios less than 2 (Figure 5G). PB-M7NIR was capable of detecting polyps of all sizes with S/R ratios remaining independent of tumor size and efficient cleavage resulting in the detection of adenomas as small as 0.01 cm^2 (Figure 5B,C,H). To determine the selectivity of the signal, APC^{Min} mice genetically deficient in

MMP7 were generated (17) and the intestines imaged with PB-M7NIR (Figure 5E). Although these mice develop less tumors due to the deficiency in MMP7, the tumors that do develop have a much lower sensor signal than WT APC^{Min} mice, and an average S/R ratio of 7 (Figure 5F–G). Statistical analysis was performed on this data using a one-way ANOVA with a Newman-Kuels multiple comparison test showing significant differences between Min and WT ($p<0.001$) as well as Min and Min-7-null ($p<0.001$) datasets, and an approximately 6-fold S/R enhancement (Min vs. Min-7-null) that can be specifically attributed to MMP7.

Ex vivo histological imaging of adenomas

To determine on a cellular level where PB-M7NIR has been activated by MMP7 in the APC^{Min} model, both whole mount and sagital sections of intestinal adenomas were imaged in the Cy5.5 (sensor) and Cy7 (reference) channels by fluorescence microscopy at 10X and 40X magnification. Fluorescence in the sensor channel localized around the adenomas in the epithelial compartment in the intestines of the APC^{Min} mice, with no signal in the lumen or in the connective tissue (Figure 6A–I). Sensor to reference ratios between seven to greater than 25 were observed in the adenomas of APC^{Min} mice (Figure 6J). As a control, normal wild type C57Bl6 mice treated with PB-M7NIR had their intestines removed and imaged in the same manner, showing limited activation of the beacon with S/R ratios less than three (Figure 6J). To confirm the presence and localization of MMP7, histochemical analysis was performed using a monoclonal antibody for MMP7. Images are shown at 40X magnification for the same sectioned adenoma verifying that MMP7 localizes to the epithelial compartment of the adenomas (Figure 4 K, L). Similar to the results with *ex vivo* IVIS imaging, the adenomas displayed an approximately 6-fold enhancement in signal that could be specifically attributable to MMP7.

Discussion

Non-invasive imaging techniques provide an extraordinary opportunity for the molecular imaging of cancer. PB-M7NIR is an enhanced version of a previously developed proteolytic nanobeacon built on a commercially available dendrimer scaffold with peptide switches selective for cleavage by MMP7 and optical sensors based on FRET (15). PB-M7NIR improves upon this previous work by utilizing near-infrared sensor and reference fluorochromes to increase the efficiency of light traveling through tissue (19). The inclusion of an internal reference fluorophore also allows for the detection of both the un-cleaved and cleaved reagent facilitating quantitative analysis and providing a much needed means to evaluate protease activity. We have demonstrated the ability of the proteolytic nanobeacon to selectively assess MMP activity using models that over-express or eliminate endogenous MMP7 activity, while the efficiency of PB-M7NIR at detecting the relatively small areas of protease activity in the APC^{Min} model demonstrates the applicability of this technology for the early detection of pre-malignant lesions.

The PB-M7NIR reagent described in the present study is comparable to protease activated NIR probes commercially available as MMPSense™ (VisEn Medical.). PB-M7NIR differs from the graft co-polymer based reagents in the PAMAM dendrimer scaffold utilized as the vehicle for circulation, the specificity of the peptide sequence, and in the use of both sensor and reference fluorophores. PAMAM dendrimers have well-defined structures that facilitate flexibility to improve the overall bioavailability of the fluorogenically labeled peptide substrates and enhance its sensitivity (30). PB-M7NIR relies on quenching of sensor fluorophores by both homotransfer self-quenching and FRET with the internal reference fluorophores. The internal reference fluorophore provides quantitative analysis of the concentration of the substrate and is useful to evaluate the pharmacokinetics of PB-M7NIR. We showed that the S/R ratios of PB-M7NIR is a useful indicator of relative MMP7 activity

in vivo, but agents such as this may be able to assess absolute levels of MMPs in normal and diseased tissue. Our further studies focus on absolute quantitative measurements of MMP activity by agents like PB-M7NIR that could be applied to human tumors.

In vivo imaging of subcutaneous xenograft tumors using PB-M7NIR showed selective imaging of MMP7 activity. In these studies, both xenograft tumors were derived from the same SW480 human colon cancer cell line expressing several MMP family members (24) and only differ in the overexpression of MMP7 in the SW480mat cells. They were injected on opposite sides of the same animal to maintain similar tumor environments and minimize animal-to-animal variation. Accumulation of biocompatible macromolecules has been reported for a variety of solid tissue tumors due to the enhanced permeability and retention effect of probes in the tumor due to leaky and constricted vasculature (31,32). The SW480 mat and neo tumors develop with consistent sizes and masses and have been shown by histological analysis to show no significant differences in vasculature (33). Therefore, the SW480neo xenograft tumors serve as an appropriate control for the SW480mat xenograft tumors from a physiological perspective. It is noted that, although the SW480neo control cells express undetectable levels of MMP7 mRNA and protein in culture (33), MMP7 can be contributed by infiltrating inflammatory cells (34). Variable levels of these host bone-marrow-derived inflammatory cells in the SW480 neo tumors may account for the variability in S/R ratios seen in tumors from the present study, and the modest average enhancement of signal in the expressing vs. non-expressing xenograft tumors as compared with the much larger difference in APC^{Min} mice with and without MMP7 expression. Host MMP7 activity can be eliminated by the use of MMP7-deficient mice, as in the APC^{Min}-7-null mice, but become more complicated for the xenograft studies that would require concomitant inactivation of the immune system to accept the human tumor xenografts.

When evaluating PB-M7NIR cleavage by MMP7 in the xenograft tumors, S/R ratios were much higher in the *ex vivo* sections than the S/R ratios seen *in vivo*, most likely due to the lack of the absorption properties of tissue and attenuation of signal due to depth of the source. The S/R ratios seen in the sections serve to localize the activation of PB-M7NIR at the cellular level, although only a small fraction of the tumor can be imaged at one time. MMP7 was found to be localized at the tumor boundary, corresponding to previous data showing MMP7 activity in macrophages (34,35), vascular endothelial cells adjacent to the tumor (36), and mononuclear phagocytes (37). Although some MMP7 activity was found within the xenograft tumors, results suggest that MMP7 predominately cleaves PB-M7NIR at the tumor-stroma interface with high activity being detected in the dermal ECM. The results suggest that MMP7 physically associates with ECM components in an active form. MMP7 may be associated with its substrates, such as the proteoglycan versican or tenascin-C (2), both which can be found in non-basement membrane matrices.

The APC^{Min} mouse provides an ideal model for evaluating the sensitivity of PB-M7NIR due to the large number of adenomas that develop in the intestinal tract at various sizes. PB-M7NIR was found to show significant sensor signal in *ex vivo* imaged adenomas as small as 0.01 cm^2 with S/R ratios being independent of tumor size. This size tumor is very difficult to detect with white light, suggesting that PB-M7NIR could be applied to enhance the detection of very small intestinal adenomas by colonoscopy. The specificity of PB-M7NIR was also demonstrated by the significant reduction in signal in all polyps of APC^{Min}-MMP7-null mice compared to APC^{Min} mice. It is not currently clear if MMP-based PBs can be sufficiently quantitative to be useful for prognostic significance, for example in distinguishing benign from malignant tumors. This application may require an absolute difference, the presence or absence of a specific MMP, rather than an alteration in the levels of expression and/or activation to be feasible.

Sagital sections of intestinal adenomas from APC^{Min} mice found effective localization of MMP7 in the epithelial compartment of the adenomas that correspond to histochemical analysis using an MMP7 antibody. At the subcellular level, we observed MMP7 staining in the basolateral region of the tumor cells. However, MMP7 activity appeared to be present throughout the cell. It is not clear if this represents the distribution of active MMP7 and/or the distribution of the product throughout the cell. It is interesting that the signal did not localize to the basement membrane or ECM between glands in the adenomas, in contrast to the abundant ECM staining in the stroma surrounding the subcutaneous tumors. This may be a result of the extreme loss of polarity with the SW480 colon carcinoma cells compared to the benign adenomas, since in cultured polarized epithelial cells MMP7 activity is primarily localized to the apical compartment (38). It is also interesting that the MMP7-attributable signal is enhanced approximately 300-fold in the xenograft tissues compared to the 6-fold enhancement in the intestinal tissues. Factors that may contribute to this difference include the overexpression of MMP7 in the SW480mat tumor cells compared to the endogenous levels of MMP7 in the adenomas, the more abundant ECM in the dermis compared to the intestine, and the possibility that there is selective retention of either the enzyme or PB-M7NIR proteolytic products by an ECM component that is differentially expressed in these tissues. Additional studies using high-resolution multi-photon microscopy are currently underway to assist in addressing these possibilities.

In summary, PB-M7NIR is the first of the dendrimeric near-infrared fluorescent probes designed for the *in vivo* detection and imaging of MMP7 activity. The intravenous administration of PB-M7NIR allowed for the sensitive and selective visualization and localization of MMP7 activity in whole animals and in tissue sections. The ability to image the tumor microenvironment may help to distinguish the specific functions of MMPs at various stages of tumor progression and in different tumor models. There remain considerable hurdles to the application of this technology to human disease, including the safety and regulatory issues surrounding the development of contrast agents for human use, the need for quantitation of absolute as opposed to relative enzyme levels, and the lack of instrumentation that is sufficiently sensitive, quantitative, and widely available for clinical use. However, these contrast agents show promise for superficial tumors or those that are accessible by endoscopy, and may be useful for the detection and prognosis of these tumors as well as in assessing response to treatment. Reagents of this type can easily be modified to image a wide variety of diseases associated with enhanced proteolytic activity.

Abbreviations

ECM	extracellular matrix
MMP	matrix metalloproteinase
PB	proteolytic beacon
NIR	near infra-red
FRET	Förster resonance energy transfer
DAPI	4',6-diamidino-2-phenylindole

Acknowledgments

This work was supported by R01 CA60867 to LMM, and the Vanderbilt-Ingram Cancer Center P30 068485. Imaging was performed at the VUIIS, SAIRP: U24 CA 126588. RLS is the recipient of an IGERT fellowship from the NSF, 0333392.

References

1. Sternlicht MD, Werb Z. How matrix metalloproteinases regulate cell behavior. Annual Review of Cell and Developmental Biology. 2001; 17:463–516.
2. Wilson, CL.; Matrisian, LM.; Parks, WC.; Mecham, RP. Matrix Metalloproteinases. San Diego: Academic Press; 1998. Matrilysin; p. 149-184.
3. Wagenaar-Miller RA, Gorden L, Matrisian LM. Matrix metalloproteinases in colorectal cancer: is it worth talking about? Cancer Metastasis Review. 2004; 23:119–135.
4. Sloane BF, Sameni M, Podgorski I, Cavallo-Medved D, Moin K. Functional imaging of tumor proteolysis. Annu Rev Pharmacol Toxicol. 2006; 46:301–315. [PubMed: 16402907]
5. Fonovic M, Bogyo M. Activity based probes for proteases: applications to biomarker discovery, molecular imaging and drug screening. Curr Pharm Des. 2007; 13:253–261. [PubMed: 17313359]
6. Weissleder R, Ntziachristos V. Shedding light onto live molecular targets. Nat Med. 2003; 9:123–128. [PubMed: 12514725]
7. Weissleder R, Tung CH, Mahmood U, Bogdanov A Jr. In vivo imaging of tumors with protease-activated near-infrared fluorescent probes. Nature Biotechnology. 1999; 17:375–378.
8. Tung CH, Mahmood U, Bredow S, Weissleder R. In vivo imaging of proteolytic enzyme activity using a novel molecular reporter. Cancer Research. 2000; 60:4953–4958. [PubMed: 10987312]
9. Petrovsky A, Schellenberger E, Josephson L, Weissleder R, Bogdanov A Jr. Near-infrared fluorescent imaging of tumor apoptosis. Cancer Research. 2003; 63:1936–1942. [PubMed: 12702586]
10. Ntziachristos V, Bremer C, Weissleder R. Fluorescence imaging with near-infrared light: new technological advances that enable in vivo molecular imaging. Eur Radiol. 2003; 13:195–208. [PubMed: 12541130]
11. Achilefu S, Jimenez HN, Dorshow RB, Bugaj JE, Webb EG, Wilhelm RR, Rajagopalan R, Johler J, Erion JL. Synthesis, in vitro receptor binding, and in vivo evaluation of fluorescein and carbocyanine peptide-based optical contrast agents. Journal of Medicinal Chemistry. 2002; 45:2003–2015. [PubMed: 11985468]
12. Achilefu S. Lighting up tumors with receptor-specific optical molecular probes. Technology in Cancer Research and Treatment. 2004; 3:393–409. [PubMed: 15270591]
13. Chen Y, Zheng G, Zhang ZH, Blessington D, Zhang M, Li H, Liu Q, Zhou L, Intes X, Achilefu S, Chance B. Metabolism-enhanced tumor localization by fluorescence imaging: in vivo animal studies. Optics Letters. 2003; 28:2070–2072. [PubMed: 14587818]
14. Jiang T, Olson ES, Nguyen QT, Roy M, Jennings PA, Tsien RY. Tumor imaging by means of proteolytic activation of cell-penetrating peptides. Proceedings of the National Academy of Sciences of the United States of America. 2004; 101:17867–17872. [PubMed: 15601762]
15. McIntyre JO, Fingleton B, Wells KS, Piston DW, Lynch CC, Gautam S, Matrisian LM. Development of a novel fluorogenic proteolytic beacon for in vivo detection and imaging of tumour-associated matrix metalloproteinase-7 activity. Biochemical Journal. 2004; 377:617–628. [PubMed: 14556651]
16. McIntyre JO, Matrisian LM. Molecular imaging of proteolytic activity in cancer. Journal of Cellular Biochemistry. 2003; 90:1087–1097. [PubMed: 14635184]
17. Tsien RY. Building and breeding molecules to spy on cells and tumors. FEBS Letters. 2005; 579:927–932. [PubMed: 15680976]
18. Pham W, Choi Y, Weissleder R, Tung CH. Developing a peptide-based near-infrared molecular probe for protease sensing. Bioconjug Chem. 2004; 15:1403–1407. [PubMed: 15546208]
19. Weissleder R. A clearer vision for in vivo imaging. Nature Biotechnology. 2001; 19:316–317.
20. Sameni M, Moin K, Sloane BF. Imaging proteolysis by living human breast cancer cells. Neoplasia. 2000; 2:496–504. [PubMed: 11228542]
21. Welch AR, Holman CM, Browner MF, Gehring MR, Kan CC, Vanwart HE. Purification of human matrilysin produced in escherichia coli and characterization using a new optimized fluorogenic peptide substrate. Archives of Biochemistry and Biophysics. 1995; 324:59–64. [PubMed: 7503560]

22. Wilson CL, Heppner KJ, Labosky PA, Hogan BLM, Matrisian LM. Intestinal tumorigenesis is suppressed in mice lacking the metalloproteinase matrilysin. Proceedings of the National Academy of Sciences of the United States of America. 1997; 94:1402–1407. [PubMed: 9037065]

23. Fingleton B, Powell WC, Crawford HC, Couchman JR, Matrisian LM. A rat monoclonal antibody that recognizes pro- and active matrix metalloproteinase-7 indicates polarized expression in vivo. Hybridoma. In Press.

24. Giambernardi TA, Grant GM, Taylor GP, Hay RJ, Maher VM, McCormick JJ, Klebe RJ. Overview of matrix metalloproteinase expression in cultured human cells. Matrix Biology. 1998; 16:483–496. [PubMed: 9550265]

25. Moser AR, Pitot HC, Dove WF. A dominant mutation that predisposes to multiple intestinal neoplasia in the mouse. Science. 1990; 247:322–324. [PubMed: 2296722]

26. Newell KJ, Witty JP, Rodgers WH, Matrisian LM. Expression and localization of matrix-degrading metalloproteinases during colorectal tumorigenesis. Molecular Carcinogenesis. 1994; 10:199–206. [PubMed: 8068180]

27. Shattuck-Brandt RL, Lamps LW, Heppner Goss KJ, DuBois RN, Matrisian LM. Matrilysin and cyclooxygenase-2 are differentially expressed in intestinal and colorectal neoplasms. Molecular Carcinogenesis. 1999; 24:177–187. [PubMed: 10204802]

28. Goss KJ, Brown PD, Matrisian LM. Differing effects of endogenous and synthetic inhibitors of metalloproteinases on intestinal tumorigenesis. International Journal of Cancer. 1998; 78:629–635.

29. Fingleton B. Matrix metalloproteinases: roles in cancer and metastasis. Front Biosci. 2006; 11:479–491. [PubMed: 16146745]

30. Boas U, Heegaard PMH. Dendrimers in drug research. Chemical Society Reviews. 2004; 33:43–63. [PubMed: 14737508]

31. Fang J, Sawa T, Maeda H. Factors and mechanism of "EPR" effect and the enhanced antitumor effects of macromolecular drugs including SMANCS. Adv Exp Med Biol. 2003; 519:29–49. [PubMed: 12675206]

32. Maeda H, Sawa T, Konno T. Mechanism of tumor-targeted delivery of macromolecular drugs, including the EPR effect in solid tumor and clinical overview of the prototype polymeric drug SMANCS. J Control Release. 2001; 74:47–61. [PubMed: 11489482]

33. Witty JP, McDonnell S, Newell K, Cannon P, Navre M, Tressler R, Matrisian LM. Modulation of matrilysin levels in colon carcinoma cell lines affects tumorigenicity in vivo. Cancer Research. 1994; 54:4805–4812. [PubMed: 8062282]

34. Haro H, Crawford HC, Fingleton B, Shinomiya K, Spengler DM, Matrisian LM. Matrix metalloproteinase-7-dependent release of tumor necrosis factor-alpha in a model of herniated disc resorption. Journal of Clinical Investigation. 2000; 105:143–150. [PubMed: 10642592]

35. Haro H, Crawford HC, Fingleton B, MacDougall JR, Shinomiya K, Spengler DM, Matrisian LM. Matrix metalloproteinase-3-dependent generation of a macrophage chemoattractant in a model of herniated disc resorption. Journal of Clinical Investigation. 2000; 105:133–141. [PubMed: 10642591]

36. Nagashima Y, Hasegawa S, Koshikawa N, Taki A, Ichikawa Y, Kitamura H, Misugi K, Kihira Y, Matuo Y, Yasumitsu H, Miyazaki K. Expression of matrilysin in vascular endothelial cells adjacent to matrilysin-producing tumors. International Journal of Cancer. 1997; 72:441–445.

37. Shapiro SD, Campbell EJ, Senior RM, Welgus HG. Proteinases secreted by human mononuclear phagocytes. Journal of Rheumatology. 1991; 18 Suppl. 27:95–98. [PubMed: 2023205]

38. Harrell PC, McCawley LJ, Fingleton B, McIntyre JO, Matrisian LM. Proliferative effects of apical, but not basal, matrix metalloproteinase-7 activity in polarized MDCK cells. Exp. Cell Res. 2005; 303:308–320. [PubMed: 15652345]

Figure 1A

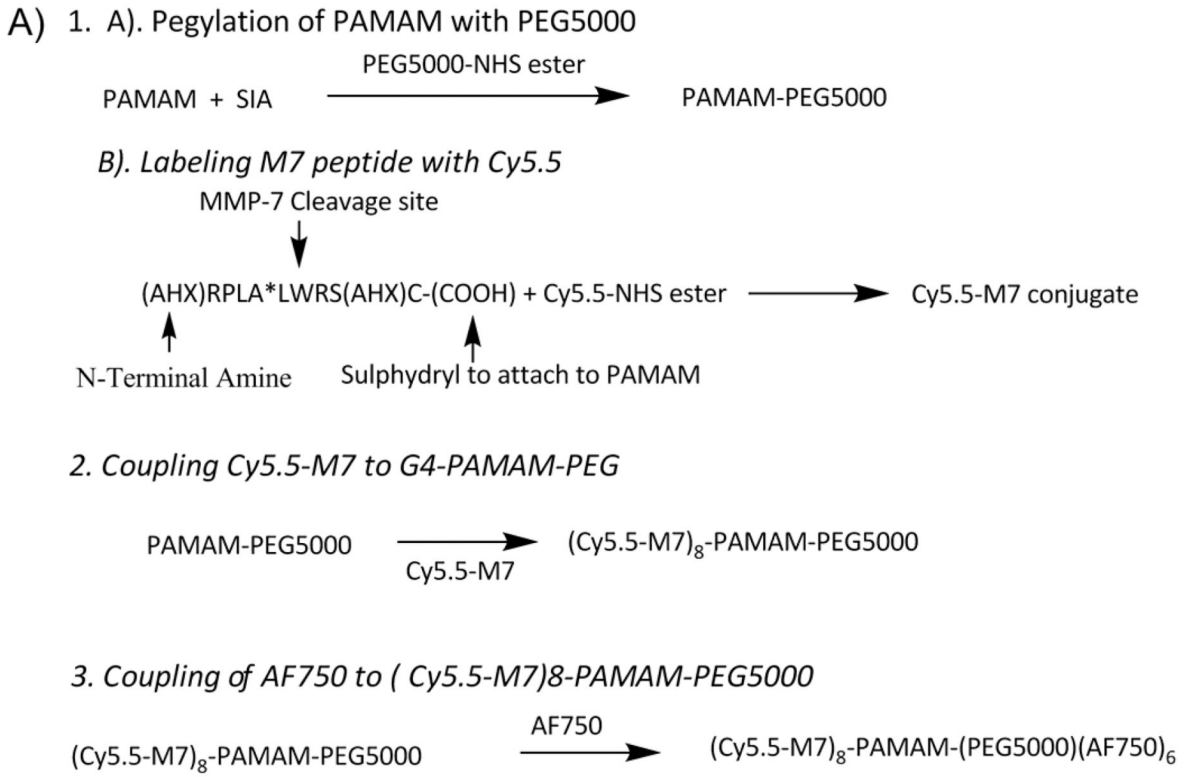

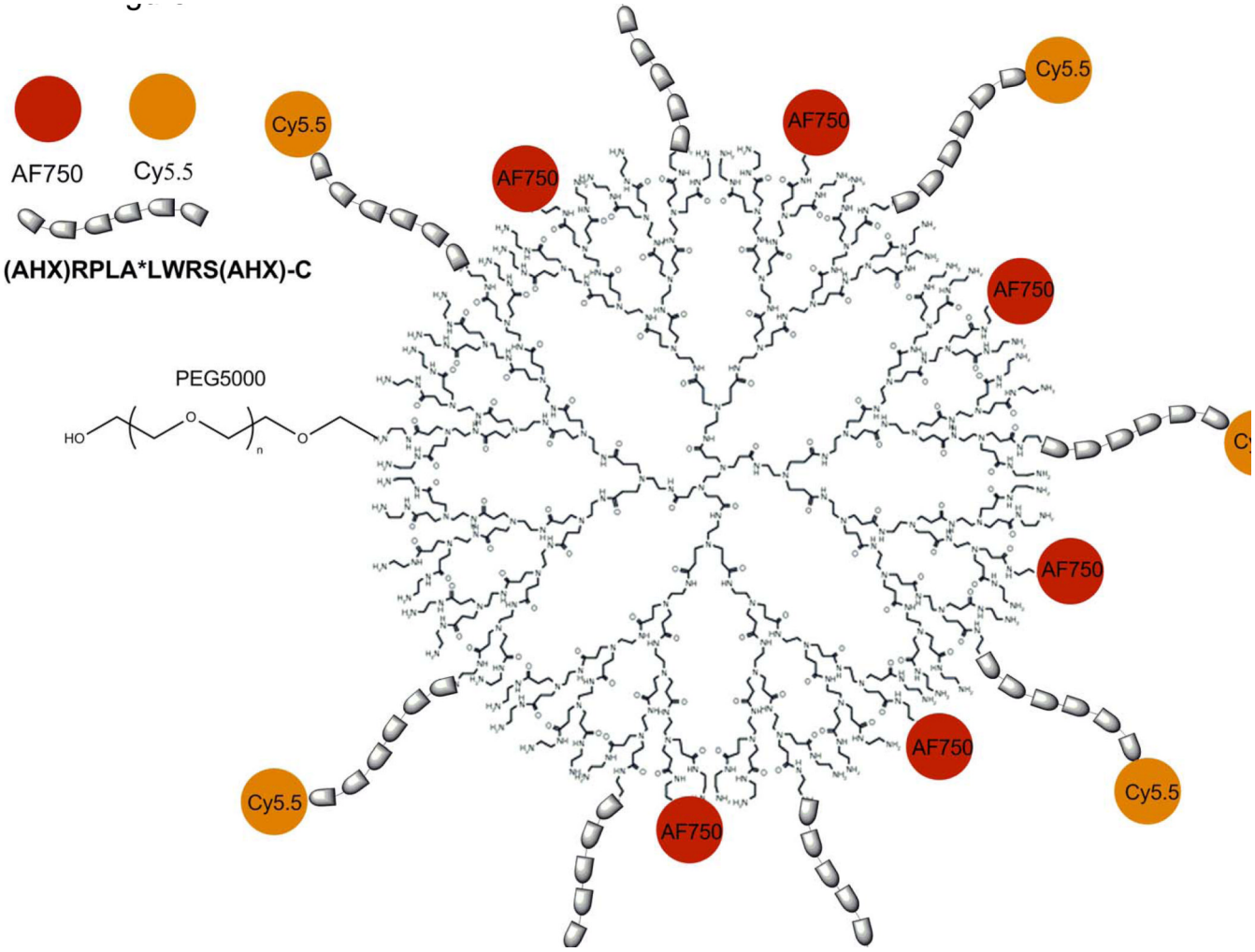

Figure 1. Synthesis and structure of PB-M7NIR

A). Scheme for the synthesis of PB-M7NIR, a (Cy5-M7)8-PAMAM-(PEG5000) (AF750)6 co-polymer. SIA = N-Succinimidyl iodoacetate B.)The Cy5.5 optical sensor is linked via AHX to the N-terminus of the MMP selective cleavable peptide (RPLA*LWRS, cleavage site denoted by asterisk) that is coupled via a second AHX and Cysteine with the PAMAM. The internal reference, AF750, of PB-M7NIR is linked directly to the dendrimer (Starburst® PAMAM dendrimer, Generation 4). Structure is not drawn to scale.

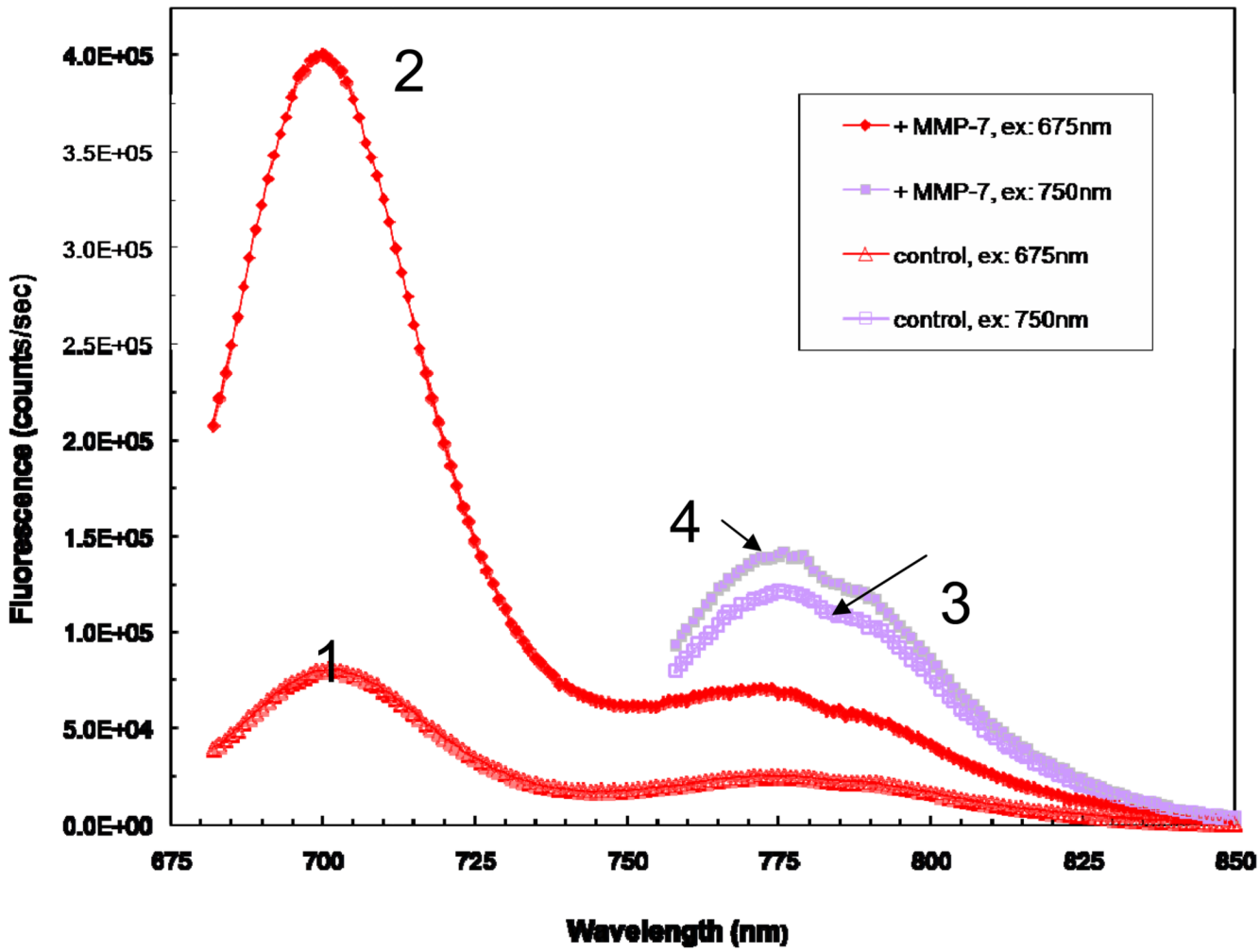

Figure 2. Fluorescence spectra for PB-M7NIR before and after MMP7 treatment

Spectra 1 represent the untreated PB-M7NIR Cy5.5-M7 peptide and spectra 3 the untreated AF750 internal reference. Spectra 2 demonstrates an approximately 5 fold increase in fluorescence of the Cy5.5 sensor post MMP7 treatment while spectra 4 demonstrates a minimal increase in fluorescence post MMP7 treatment.

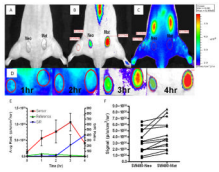

Figure 3. In vivo imaging of mouse subcutaneous xenograft tumors with PB-M7NIR

Dorsal, caudal view of a nude mouse 4 weeks following subcutaneous injection of SW480neo (Neo) or SW480mat (Mat) cells. Tumor areas (approximately 57mm2 each) are shown in white light (A), the Cy5.5 Sensor channel (B), and the ICG Reference channels (C) 4 hr post retro-orbital intravenous injection of 1.0 nmole PB-M7NIR. Encircled areas represent regions of interest for quantitative assessment. Note accumulation of PB-M7NIR in the kidneys of the mouse as detected with the ICG reference channel (C), but selective accumulation of sensor signal in the Mat tumor indicative of proteolytic activity (B). Sensor signal on the spine and tail are presumed to be due to low levels of circulating, activated probe that become detectable when they are close to the surface of the mouse. (D) Higher magnification of the sensor signal images of the Neo and Mat tumors of the same mouse at 1, 2, 3, and 4h timepoints. (E) Sensor (red squares) and reference (green triangles) signals plotted over time in a mat tumor showing increased signal in the sensor channel starting at the 2 hr time point reaching a maxima at the 3–4 hr imaging point. S/R ratio (blue inverted triangles) increases with time. Mean and Standard Deviation, n=3 (F) Sensor signal in the SW480neo and SW480mat tumor for each individual mouse is indicated by the linked symbols (n=13).

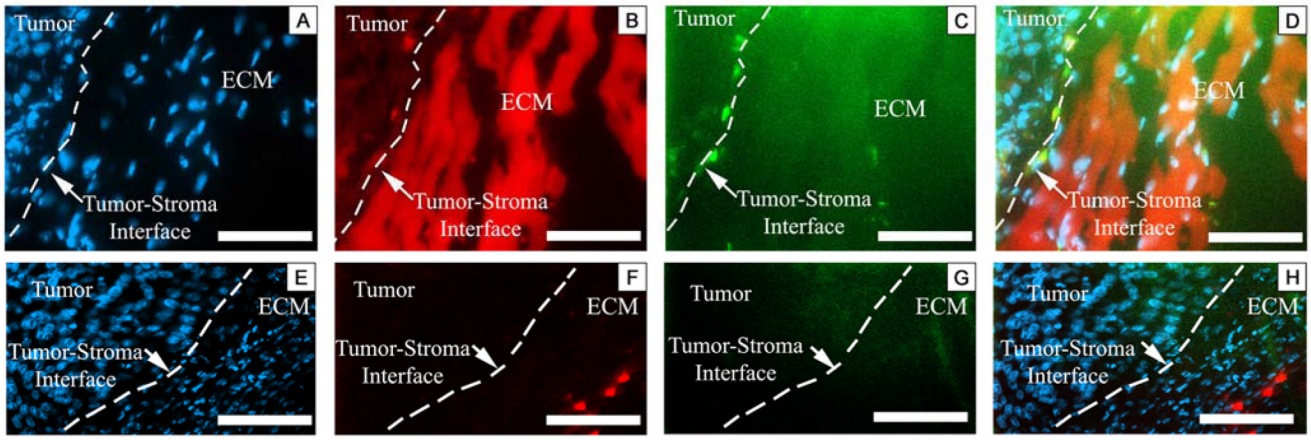

I

Mouse	Neo Tumor Sensor (x10^6)	Neo Tumor Reference (x10^6)	Neo Tumor S/R	Mat Tumor Sensor (x10^6)	Mat Tumor Reference (x10^6)	Mat Tumor S/R	Mat/Neo
M# 1	45 ± 7.2	11 ± 1.2	2.0 ± 0.8	270 ± 41	5.5 ± 8.3	687 ± 234	340
M# 4	44 ± 10	24 ± 0.2	1.8 ± 0.2	240 ± 48	4.3 ± 1.9	1020 ± 503	567
M# 7	120 ± 20	31 ± 0.4	4.2 ± 0.9	280 ± 13	0.5 ± .07	571 ± 22	136
M# 12	37 ± 1.8	28 ± 0.9	1.3 ± 0.3	290 ± 61	0.6 ± 0.4	492 ± 92	378
			Avg = 2.3			Avg = 692	Avg = 355

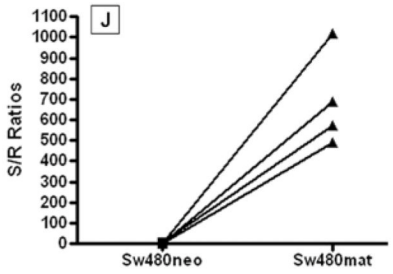

Figure 4. Histological imaging of PB-M7NIR in xenograft tumors

SW480mat (A–D) and SW480neo (E–H) xenograft tumors were harvested post injection of PB-M7NIR at 4 hr and frozen in OCT, sectioned, and stained with DAPI. Images taken with the Axiophot fluorescent microscope, 40X, white dash =50 microns. A&E) DAPI channel depicts cell nuclei in blue, B&F) Sensor Channel (peak emission 694 nm) demonstrating activated PB-M7NIR in red, C&G) Reference channel (peak emission 776 nm) showing PB-M7NIR in green (reference signal presumed to be due to macrophage uptake of PB-M7NIR), D&H) Merge of the images in A–C and E–G, respectively. The dotted lines indicate the boundry between the highly cellular tumor and the less cellular stromal, ECM-rich region. I). Sensor, Reference, and S/R ratio values from the integrated background-corrected intensities for neo and mat tumors from 4 individual mice. Images from each tumor were taken in triplicate and mean +/− SD are shown. (J) Plot of the S/R ratios for the neo and mat tumor from each mouse.

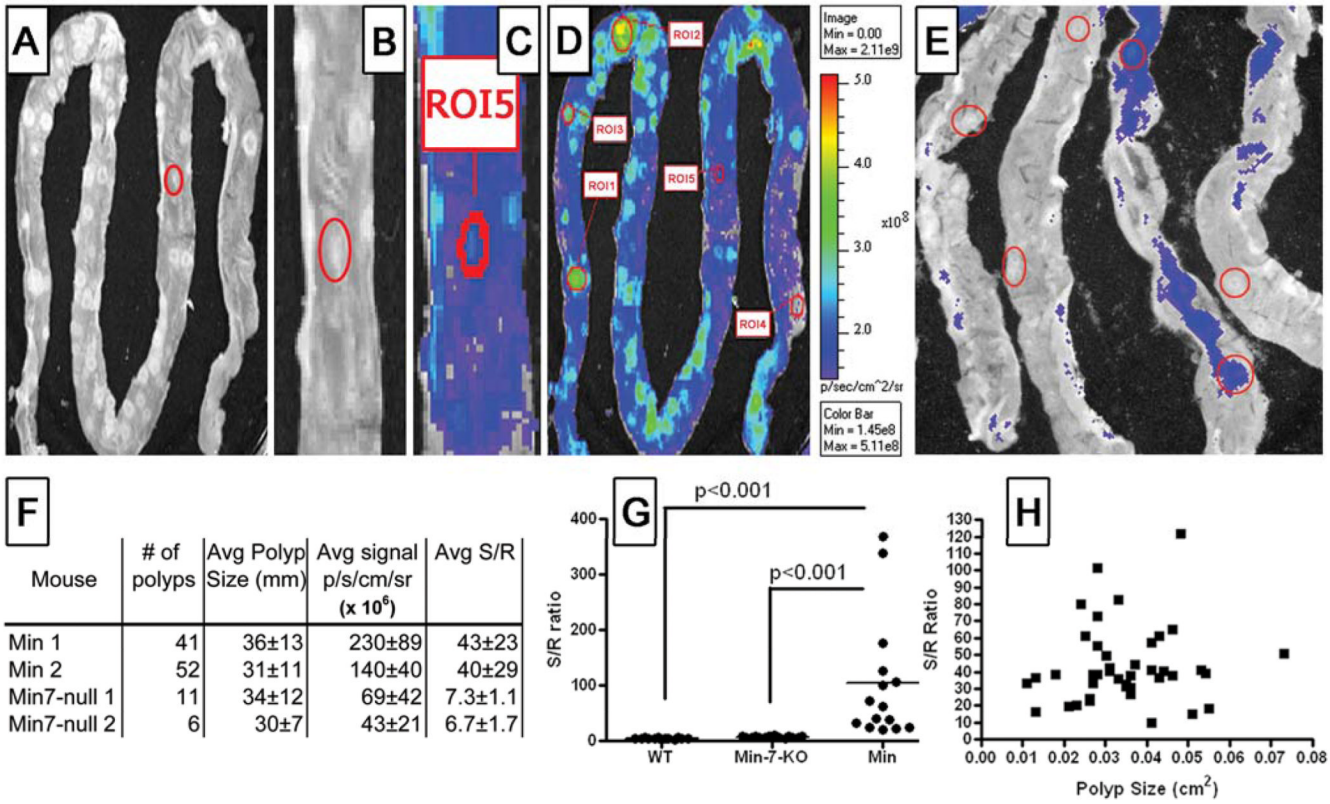

Mouse	# of polyps	Avg Polyp Size (mm)	Avg signal p/s/cm/sr (x 10^6)	Avg S/R
Min 1	41	36±13	230±89	43±23
Min 2	52	31±11	140±40	40±29
Min7-null 1	11	34±12	69±42	7.3±1.1
Min7-null 2	6	30±7	43±21	6.7±1.7

Figure 5. Ex vivo imaging of PB-M7NIR in APC^{MIN} intestinal adenomas

Explanted mouse intestine from an APC^{MIN} mouse with spontaneous polyps 60 min. post-injection of 1nmole of PB-M7NIR Beacon. A&B) White light images C&D) NIRF image in the Cy5.5 (sensor) channel. ROI = region of interest B&C) Higher magnification of ROI 5 (Red circle in panels A–C). E) Sensor channel image of intestines from APC^{Min}/MMP7-null mouse 1h post-injection of 1nmole of PB-M7NIR Beacon. Polyps are circled in red. F) Table of data from individual mice showing the number of polyps/mouse, the polyp size (mean +/− SD) the Sensor signal (Mean +/− S.D.), and the S/R ratios (Mean +/−S.D.). (n= the number of detectable polyps.) (G) S/R ratios for random ROIs from the intestine of 2 wild-type mice (WT, n=4), and adenomas from 2 individual APC^{Min}/MMP7-null mice (Min-7-null, n=4), and 2 APC^{Min} mice (Min-WT, n=4). p<0.001, one-way ANOVA H) S/R Ratios are plotted versus tumor size. The correlation coefficient r_{xy}, <0.1; (n=4 mice), is considered to show no evidence of a correlation between the x and y axis.

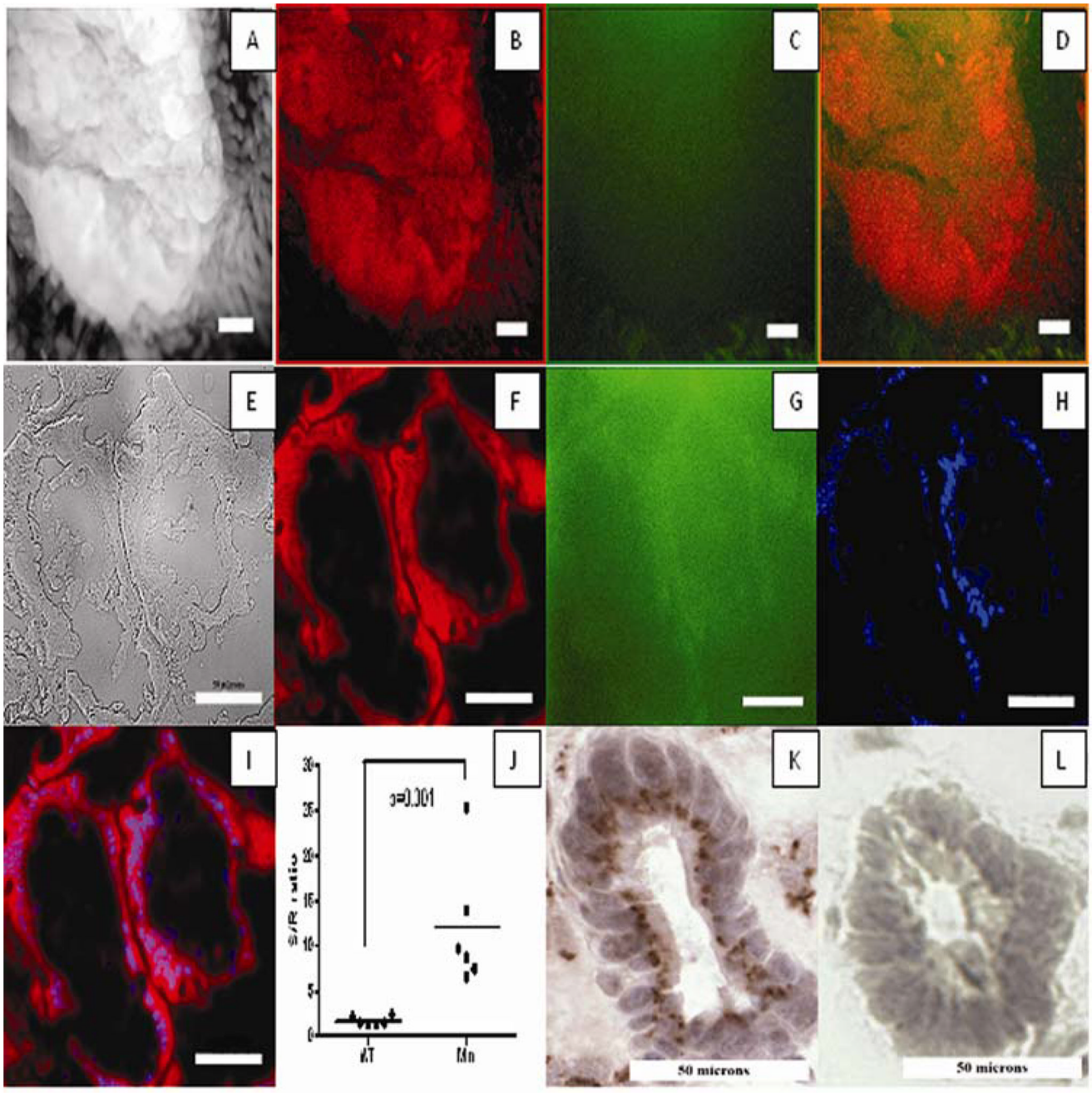

Figure 6. Histological imaging of PB-M7NIR in APC^{MIN} adenomas

Images of a single, intact adenoma (A–D, 10X-objective) and a sagital frozen section (E–I, 40X-objective) of the same intestinal adenoma from an APC^{Min} mouse, showing two distinct glandular structures within the adenoma, each with a central lumen. A frozen section from a single glandular structure in the same adenoma at higher power shows a ring of epithelial cells around a central lumen (panels K–L). Staining with an MMP7 antibody (panel K) shows the enzyme is concentrated in an intracellular structure on the luminal side of the epithelial cells. A&E) White light, B&F). False-red coloring in the Cy5.5 (sensor) channel C&G) Cy7 (Reference-green) channel. D). Merge of images from both Cy5.5 and Cy7 channels H) DAPI (blue) signal showing the nuclei of cells, in particular the nuclei at

the base of the epithelial cells that form adenoma glandular structures. I). Merge of images from the Cy5.5, DAPI, and Cy7 channels J). Quantitative fluorescent images were analyzed using Metamorph software with intensities recorded in counts/sec. Sensor to Reference ratios were calculated after background subtraction K&L). Immunohistochemical staining of the same adenoma with a specific anti-MMP7 monoclonal antibody (K) or an IgG control antibody (L), detector = brown precipitate. A–D white line=100 microns; E–I, K–L white line=50 microns.

Table 1

Fluorescence Imaging Detection of PB-M7NIR in vivo

Fluorescence intensities (photons/sec/cm2/steradian) measured in the Cy5.5 (signal) and ICG (reference) channels (n=13) of images containing anesthetized live mice carrying bilateral xenograft tumors (SW480neo and SW480mat). Regions of interest were drawn around the tumors and results are expressed in avg. radiance after correction for background signal. Results were taken at the 4 hr time point post injection of PB-M7NIR with sensor/reference ratios determined for each tumor with an average (Mat tumor S/R)/(Neo tumor S/R) of 6.87 with a median of 2.2.

Mouse	Neo Tumor				Mat Tumor				
	Tumor Size (cm)	Signal (p/s/cm/sr)	Reference (p/s/cm/sr)	S/R Ratio	Tumor Size (cm)	Signal (p/s/cm/sr)	Reference (p/s/cm/sr)	S/R Ratio	Mat S/R Neo S/R
1	1.10	6.75E+06	6.47E+06	1.04	0.80	3.40E+08	7.34E+06	46.3	44.5
2	0.88	4.14E+08	2.00E+07	24.3	0.46	4.87E+08	1.20E+07	34.5	1.42
3	0.70	9.40E+07	1.70E+07	5.54	0.71	4.90E+08	1.43E+07	34.3	6.19
4	0.71	1.19E+08	1.60E+06	74.3	0.70	1.74E+08	1.50E+05	1160	15.6
5	0.58	1.69E+08	2.24E+06	75.4	0.82	2.61E+08	9.10E+05	287	3.80
6	1.20	1.82E+08	6.38E+06	28.5	0.81	3.14E+08	5.58E+06	57.0	2.00
7	0.29	6.15E+07	3.50E+06	17.6	0.83	1.38E+08	9.90E+06	39.3	2.24
8	0.35	8.33E+07	3.74E+06	19.7	0.46	8.97E+07	4.22E+06	24.0	1.22
9	0.19	1.06E+08	3.60E+05	293	0.31	2.93E+08	1.17E+05	1150	3.93
10	0.21	8.59E+07	4.30E+06	199	0.32	1.87E+08	4.30E+06	435	2.18
11	0.29	3.49E+08	4.07E+06	85.8	0.23	4.54E+08	4.02E+06	113	1.32
12	0.34	1.72E+08	4.37E+06	39.2	0.28	3.73E+08	2.72E+06	137	3.49
13	0.58	1.76E+08	4.12E+06	42.6	0.81	2.33E+08	3.83E+06	60.8	1.43
				Avg.=69.7				Avg.=275	Avg.=6.87

Mol Imaging. Author manuscript; available in PMC 2009 November 16.